Role of negative electrode porosity in long-term aging of NMC//Graphite Li-Ion batteries

P. Bernard, Hervé Martinez, C. Tessier, E. Garitte, S. Franger, Rémi Dedryvère

Role of negative electrode porosity in long-term aging of NMC//graphite Li-ion batteries

Pierre BERNARD,[a,b] Hervé MARTINEZ,[a,d] Cécile TESSIER,[c,d] Emmanuelle GARITTE,[c,d] Sylvain FRANGER,[b,*] Rémi DEDRYVERE [a,d,*]

[a] IPREM, University of Pau, CNRS (UMR 5254), Hélioparc, 2 avenue Pierre Angot, 64053 Pau Cedex 9, France
[b] ICMMO/ERIEE (UMR CNRS 8182), University Paris Sud, University Paris-Saclay, 15 Avenue Georges Clemenceau, 91405 Orsay, France
[c] SAFT, 111-113, Boulevard Alfred Daney, 33074 Bordeaux Cedex, France
[d] Réseau sur le Stockage Electrochimique de l'Energie (RS2E), FR CNRS 3459, France

Abstract

Electrochemical energy storage associated to renewable energy sources requires devices with very long lifespan. In this work we simulated the long-term aging of $Li(Ni_{2/5}Mn_{2/5}Co_{1/5})O_2$ (NMC) // graphite lithium-ion batteries by standardized accelerated aging tests in tough storage and cycling conditions. Aging mechanisms taking place at the graphite electrode/electrolyte interface were characterized by X-ray Photoelectron Spectroscopy (XPS) and Electrochemical Impedance Spectroscopy (EIS). Besides usual aging processes commonly admitted, we highlight the role of electrode porosity. A model is proposed to describe the electrical behavior of the electrodes taking into account the influence of electrochemically blocking pores. The blocking effect of pores is believed to be caused by confinement of Li_2CO_3 and/or gaseous CO_2 inside the narrow pores, which do not allow lithium ions to diffuse and insert into graphite. In these pores, lithium can only participate to SEI growth which decreases the capacity by lithium consumption.

Keywords: Lithium-ion batteries, XPS, EIS, graphite, interface, SEI, porosity

* corresponding authors (sylvain.franger@u-psud.fr, remi.dedryvere@univ-pau.fr)

1. Introduction

The development of wide-scale renewable energy production such as wind and solar energy is strongly linked with the concern of electrical energy storage. An efficient storage is necessary for an optimized use of these power sources as they are by nature intermittent and often unpredictable [1]. This leads to a mismatch between energy production peaks and consumption peaks [2]. Thus, efficient storage systems are required in order to keep the energy produced for a high energy demand period. However, this application requires long lifetimes for cost and maintenance reasons. Among electrochemical storage devices, Li-ion secondary battery technology appears to be a good candidate [3,4] displaying good cycle life, low self-discharge and good reliability. Li-ion batteries for common applications such as mobile electronic devices or HEV/EVs are usually planned to last about 3 and 10 years, respectively [5,6], but renewable energy storage requires at least a 15 to 20 years lifespan to be economically viable. Li-ion accumulators seem suitable and promising for this particular application field [7,8]. Such a long-term use of accumulators has obviously aging consequences and various phenomena are known to cause battery performances fading. Ten years ago already, Vetter et al. [9] and Broussely et al. [10] proposed an overview of aging mechanisms occurring in Li-ion batteries such as active material cracking [11] or degradation by metal dissolution [12,13], binder decomposition, current collector corrosion [14].

Negative electrode aging especially has been extensively studied and reviewed [15]. Graphite is the most widely used negative electrode material in Li-ion technology. It is already known to be affected by changes at the electrode/electrolyte interface, aging of the active matter and of the other components (binder, current collector, conductive additives…) [9], leading to capacity loss and impedance rise. Electrode/electrolyte interface is often considered to be the main location of aging mechanisms for the negative electrode. To summarize, SEI (Solid Electrolyte Interphase) growth [16] or instability [17], lithium plating, and graphene planes exfoliation by solvent co-intercalation are believed to be the main aging mechanisms [18] for negative electrodes. Bulk aging caused by structural changes are considered to be of much lower influence. This demonstrates the importance of electrode/electrolyte interfaces and of the SEI in Li-ion cells aging.

Li-ion batteries long-term aging has been widely studied for the automotive applications (EV/HEV) [19,20,21]. For example, phenomenological models have been developed for this application based on Buttler-Volmer equations and experimental data [22,23]. Numerous aging prediction models were developed for Li-ion secondary batteries [24,25,26]. Most of the studies considering both negative and positive electrodes report that aging effects result in the loss of electrochemically active lithium upon cycling, leading to the decrease of the lithium insertion in the positive electrode

material [10]. Generally, studying aging mechanisms in Li-ion batteries often faces a critical difficulty: different aging mechanisms are known to occur at the same time and mechanisms are often not independent, which makes the identification of a particular mechanism as well as its causes difficult to identify [9,27].

In the present study we simulated the long-term aging of $Li(Ni_{2/5}Mn_{2/5}Co_{1/5})O_2$ (NMC) // graphite full cells. In order to study the long-time aging of the batteries in a reasonable time scale, accelerated electrochemical tests were performed under tough conditions, in order to simulate a longer operational use in normal conditions. Two different aging tests were performed: *(i)* keeping the cells at high potential, full state of charge (SOC) during several months at 60°C to simulate a storage/calendar aging, and *(ii)* cycling the cells at full voltage range with a fast cycling rate at room temperature. We focused on aging processes taking place at interfaces. Therefore this study was carried out by X-Ray photoelectron spectroscopy (XPS) and Electrochemical Impedance spectroscopy (EIS), which are complementary techniques which give access to very different kinds of information on the interfaces. EIS also allows the study of bulk phenomena due to the large frequency band scanned. Positive and negative electrodes were both analyzed but the discussion is here focused on the negative electrodes. We show that the porosities of the negative electrodes play a major role in aging processes at interfaces, that is not sufficiently taken into consideration to have a complete overview on aging mechanisms.

2. Experimental conditions

2.1. Accelerated aging

The positive electrode was composed of the layered oxide $Li(Ni_{2/5}Mn_{2/5}Co_{1/5})O_2$ (NMC), carbon black as electronic percolant and PolyVinylidene Fluoride (PVdF) as mechanic binder. This mixture was deposited on an aluminum foil as current collector, in order to obtain a loading of 30 $mg.cm^{-2}$. The negative electrode consisted of graphite with the binders CMC (carboxymethyl cellulose, Na salt) and SBR (Styrene Butadiene Rubber) deposited on a copper current collector. The electrolyte was composed of $LiPF_6$ (1 $mol.l^{-1}$) dissolved in a mixture of 70% vol. of linear carbonates and 30% vol. of cyclic carbonates. Vinylene carbonate (VC) was used as electrolyte additive (3%). Each accumulator consisted of a cylindrical element (d=12 mm, h=60mm) with a capacity of 4.2 Ah.

The first cycle was carried out at 60°C between 2.7 V and 4.1 V at C/5 rate. The batteries, after this first cycle and after an additional control cycle in the same conditions, were used as a reference to compare with aged batteries. The cells were submitted to the following accelerated aging conditions:

(i) Storage/calendar aging: the cell is kept at charged state during 3 months at 60°C (4.1 V). Each time the potential decreases below 4.03 V, the battery is charged again up to 4.1 V
(ii) Cycling aging: 490 cycles at C rate between 2.7 V and 4.1 Vat room temperature.
After discharge at 2.7V, the batteries were opened in a dry argon glove box and the aged electrodes were rinsed 3 times with DMC before XPS or EIS analysis.

2.2. X-ray Photoelectron Spectroscopy (XPS)

XPS analysis was performed using a Kratos Axis-Ultra spectrometer with a monochromatized X-ray source (Al Kα: hv=1486.6 eV). The analysis chamber is under ultra-high vacuum (< 1.10^{-6} Pa). The analysis area is 300×700 µm². Peaks were recorded at pass energy 20 eV. Quick test spectra were recorded before and after the acquisition of high resolution spectra, in order to check for eventual sample degradation due to X-ray beam exposure. No degradation was observed. In order to preserve the samples from air and moisture, they were prepared in dry argon atmosphere. The argon glove box is coupled to the spectrometer. This way, air exposure is avoided for all analysis steps: from battery opening to XPS measurement. Peaks were fitted using the Casa XPS software (with a 70% Gaussian and 30% Lorentzian peak shape) and binding energies are calibrated according to the contamination hydrocarbon C 1s peak location set at 285 eV.

2.3. Electrochemical Impedance Spectroscopy (EIS)

The EIS measurements were carried out either with 2-electrode or 3-electrode cells. Swagelok 2-electrode symmetric configuration cells lead to EIS spectra displaying exclusively the impedance response of the sample, but they do not allow changing the lithiation state of the samples. For this particular purpose a 3-electrode cell with Li^0 for both the counter and the reference electrodes was used. Both type of cells were assembled in a glove box under dry argon atmosphere to avoid air and moisture exposure. The electrolyte used was a standard LP100 (1M $LiPF_6$ in EC/PC/DMC 1/1/3 mixture) electrolyte provided by Merck. Impedance spectra were then recorded with a VMP-3 BioLogic multipotentiostat, using EC-Lab as acquisition software. The excitation signal had an amplitude of 20 mV peak to peak in a frequency range from 100 kHz to 63 mHz. Three measurements were performed per frequency and 13 points were recorded per decade. The resulting spectra were fitted using the ZView2 software from Scribner® and minimizing differences with impedance modulus according to a weighted least square method. All experiments were performed in a room constantly kept at 25°C to get rid of impedance variations resulting from possible temperature changes.

3. Results and discussion

Figure 1 displays the evolution of the battery capacity during accelerated storage (Figure 1a) and accelerated cycling (Figure 1b) aging. The capacity is expressed as a percentage of the initial capacity (4.2 Ah) of the accumulator. After 97 days of storage at 60°C, the battery capacity decreased by 6%. After 490 cycles at C rate at room temperature the battery lost 6% of its original capacity. The negative electrodes recovered from the batteries after 97 days of storage and 490 cycles at C rate were used for the following characterizations.

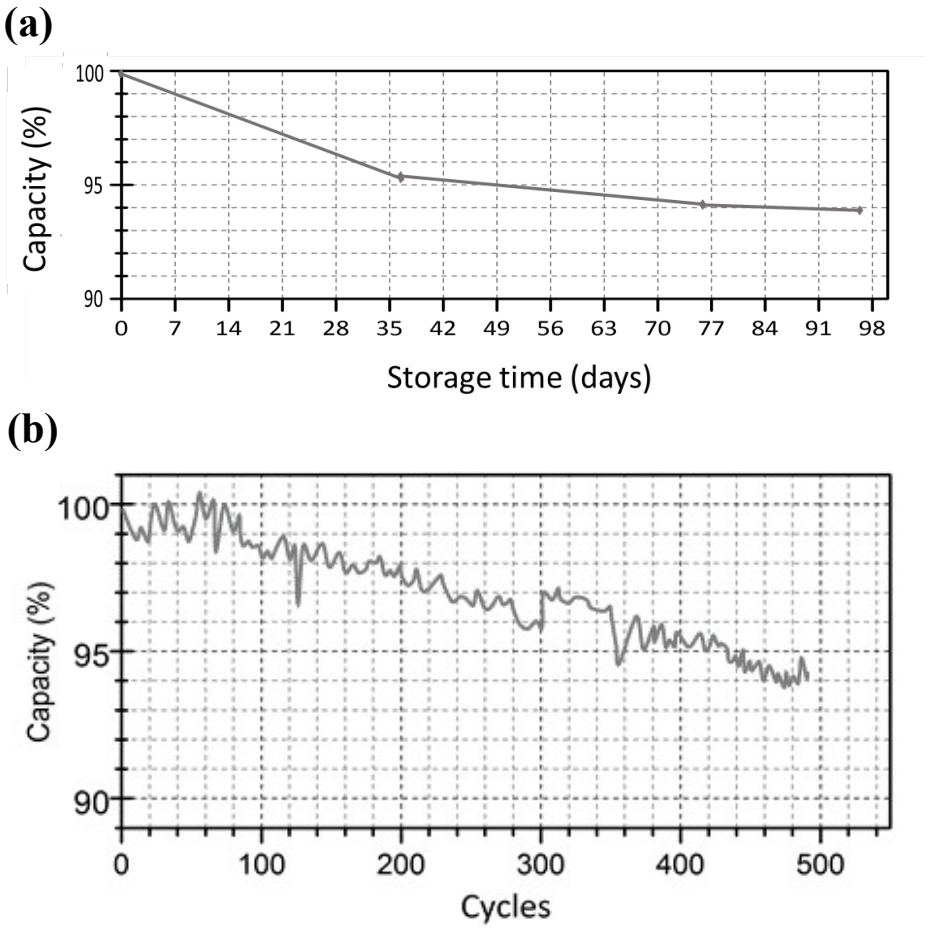

Figure 1: Evolution of the discharge capacity of NMC//graphite full cells through accelerated aging tests with respect to the initial capacity (4.2 Ah): **(a)** storage at charged state (4.1 V) during 3 months at 60°C ; **(b)** Cycling at C rate between 2.7 and 4.1 V at room temperature.

3.1. Surface chemical characterization(XPS)

C 1s core peaks

The C 1s spectrum of the pristine graphite electrode (Figure 2) is consistent with the expected profile for similar electrodes [28,29]. It displays a narrow peak at 284 eV corresponding to graphite. Mechanical binders C 1s contributions also appear in the spectrum: the peak located at 285 eV is attributed to the Styrene-Butadiene Rubber (SBR) as well as hydrocarbon contamination; the two following peaks at higher binding energy (286.7 eV and 288.4 eV) are assigned respectively to CO and COO carbon environments from the CMC binder [28]. A low intensity peak around 291 eV is also detected corresponding to the shake-up satellite caused by π-π* transitions and also plasmons of graphite.

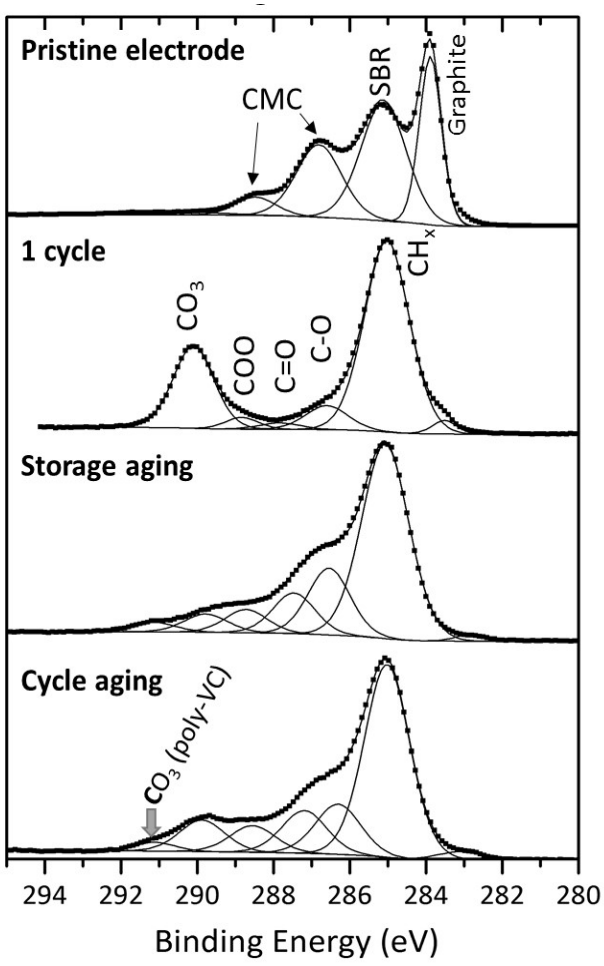

Figure 2: XPS C 1s core peaks of negative electrodes: pristine composite electrode, after a first cycle (formation + control), after storage and cycling accelerated aging tests.

After a first cycle at 60°C, the spectrum shows a significantly different profile: the graphite contribution is now hardly visible, showing the formation of the solid electrolyte interphase (SEI). Considering the detection of a very small amount of graphite, the thickness of this layer can be estimated close to 5 nm, in regard to the typical XPS probing depth. An additional peak is detected at 290 eV revealing the presence of CO_3 environments (carbonate) at the surface of the sample due to electrolyte solvents degradation products such as $ROCO_2Li$ and Li_2CO_3 [29,30]. The other peaks located at 286.7 and 288.8 eV are no longer attributed to CMC but to other species resulting from electrolyte solvents degradation. These new peaks correspond to the presence of compounds deposited at the surface of the sample and constituting the SEI, which contains CH, CO, COO and CO_3 environments of carbon according to Figure 2. As the C-O/CO_3 intensity ratio is low, most of the carbonate signal is due to Li_2CO_3. In this case, the amount of carbonates (mainly Li_2CO_3) at the surface of the graphite electrode reaches more than 40 at. %.

After aging tests, either in storage or cycling mode, one can notice that the SEI contains less carbonates than after the first cycle (around 15 at. % and 24 at. %, respectively). An additional weak peak at high binding energy (~291eV) can be detected. Only few carbonated species display such a high binding energy. This peak is attributed to lithium-free CO_3 environments typical from the polymer ensuing from VC additive degradation at the surface (polyVC) as demonstrated in a previous work [31]. This is in good agreement with corresponding O 1s spectra showing a peak at 534.5 eV with a O 1s/C 1s ratio close to 2 attributed to C-O (not shown here). We note that CO_3-like carbons from polyVC were not detected after a first cycle, which is still in accordance with O 1s corresponding spectrum.

F 1s and P 2p core peaks

F 1s spectra (Figure 3a) display two peaks at 687 and 685 eV, respectively. The first one is attributed to $LiPF_6$, either from salt traces remaining after the rinsing process, or PF_6^- ions as integral part of the SEI. The second peak is attributed to LiF, which is the main degradation product of $LiPF_6$. Table 1 summarizes the quantities (in atomic percentage) of lithium salts detected at the surface of the graphite electrodes. After a first cycle, the LiF quantity is 3 at.% (including Li). The negative electrodes from the aged cells display a quantity of 3 at.% of LiF after storage and 2.2 at.% after cycling. It can be thus concluded that the salt does not degrade significantly upon accelerated aging tests. The overall degradation of the electrolyte (including solvents) appears to be globally limited.

In corresponding P 2p spectra (Figure 3b), each phosphorous contribution consists of a doublet of non-resolved peaks due to spin-orbit coupling (P $2p_{3/2}$and P $2p_{1/2}$ with 2/1 intensity ratio). The highest binding energy doublet located at 137.2 eV is assigned to $LiPF_6$ (and/or or PF_6^- ions) and is

in good accordance (intensity ratio) with the corresponding F 1s peak at 687.0 eV. The second doublet, around 134.2 eV is assigned to phosphates coming from degradation of the salt. The two graphite electrodes after storage and cycling aging tests display limited amounts of phosphates (2-3 at. % of PO_4, including oxygen). The slight decrease of the binding energy of the other peak (136.6 instead of 137.2 eV) may be due to the presence of partially degraded $Li_xPF_yO_z$ compounds at the surface.

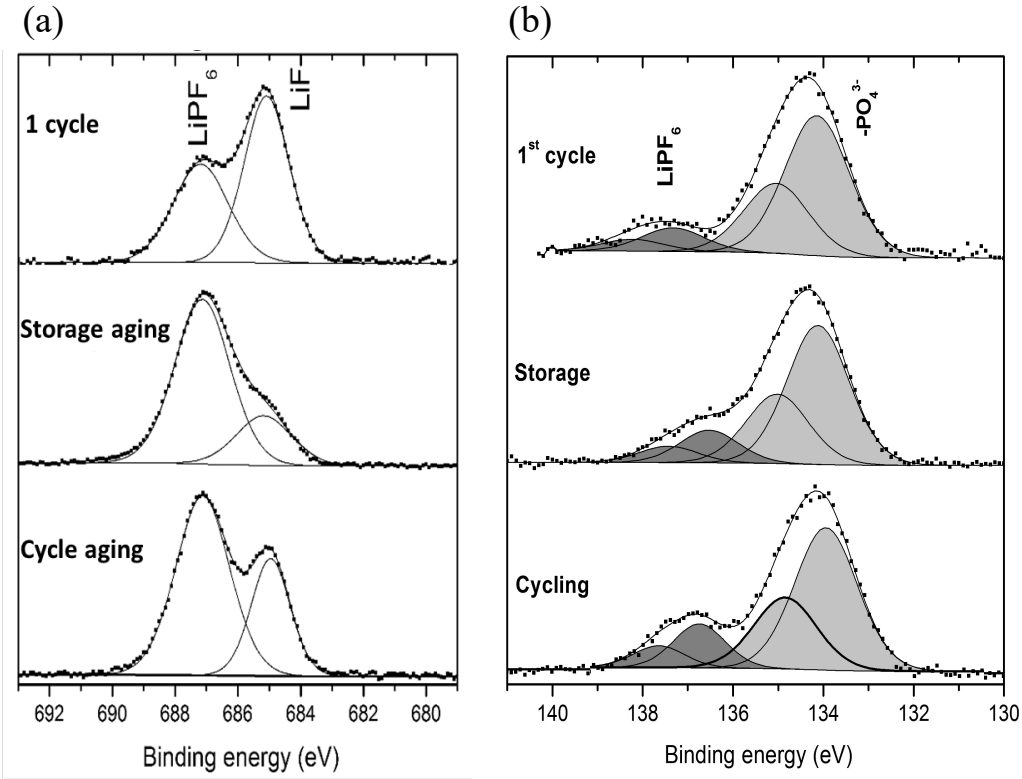

Figure 3: **(a)** F 1s and **(b)** P 2p core peaks of negative electrodes after a first cycle (formation + control), after storage and cycling accelerated aging tests.

Table 1: Quantities of lithium salts detected at the surface of the electrodes by XPS

	1st cycle	**Storage aging**	**Cycling aging**
Inorganic carbonates	48 at. %	15 at. %	24 at. %
$LiPF_6$	1.5 at. %	5.3 at. %	2.8 at. %
LiF	3 at. %	3 at. %	2.2 at. %

To sum up, the batteries display a good capacity retention for both storage and cycling aging tests. Electrolyte salt degradation products such as phosphates or LiF are globally detected in rather low quantities, even after storage at 60°C. One can assume that the electrolyte salt degradation is then limited during extended aging. Cycling aging generates slightly higher quantities of carbonates in the SEI than storage. SEI thickness seems close to the XPS probing depth (~5 nm), however the small quantity of graphite still detected at the surface may be due to areas displaying locally thinner SEI and/or holes in the film. Information provided by EIS is useful in this case in order to provide additional information on the SEI.

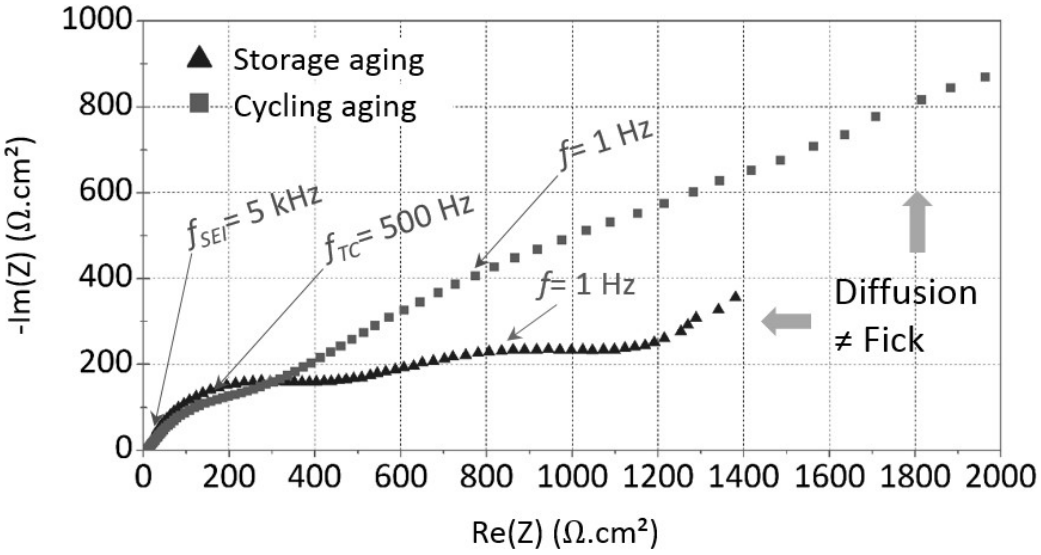

Figure 4: EIS Nyquist plots of graphite electrodes after storage and cycling accelerated aging tests. Characteristic frequency values are indicated on the figure.

3.2. Electrical characterization of the interphase (EIS)

Figure 4 shows the EIS Nyquist plots of the negative electrodes. The exploitation of these spectra is quite complex due to their unusual profile: there is indeed no clear resolved contribution corresponding to charge transfer and the Warburg region (corresponding to the semi-infinite diffusion phenomenon) is depressed. However, the high frequency part of the spectrum (5 kHz) corresponding to the contribution of the SEI can be modeled conventionally. After only one control cycle, the SEI resistance (R_{SEI}) was close to 10 Ω.cm². Aging processes contribute to drastically increase the R_{SEI} value: 90 Ω.cm² after cycling and 130 Ω.cm² after storage. Besides, XPS C 1s spectra have shown no significant differences in terms of SEI thickness since the signal of the

graphite active material was rather similar for aged electrodes compared to the sample after a first cycle. Therefore we can assume that the significant R_{SEI} difference measured by EIS is driven by the morphology and density of the SEI rather than by its thickness. The low frequency part of the EIS spectra is more difficult to interpret (~1 Hz). The particular shape of these spectra may be due to the contribution of the porosity of electrodes. Therefore, we checked the porosity of the graphite negative electrodes by Scanning Electron Microscopy (SEM) coupled with Focused Ion Beam (FIB) allowing to cut a cross section of the electrode.

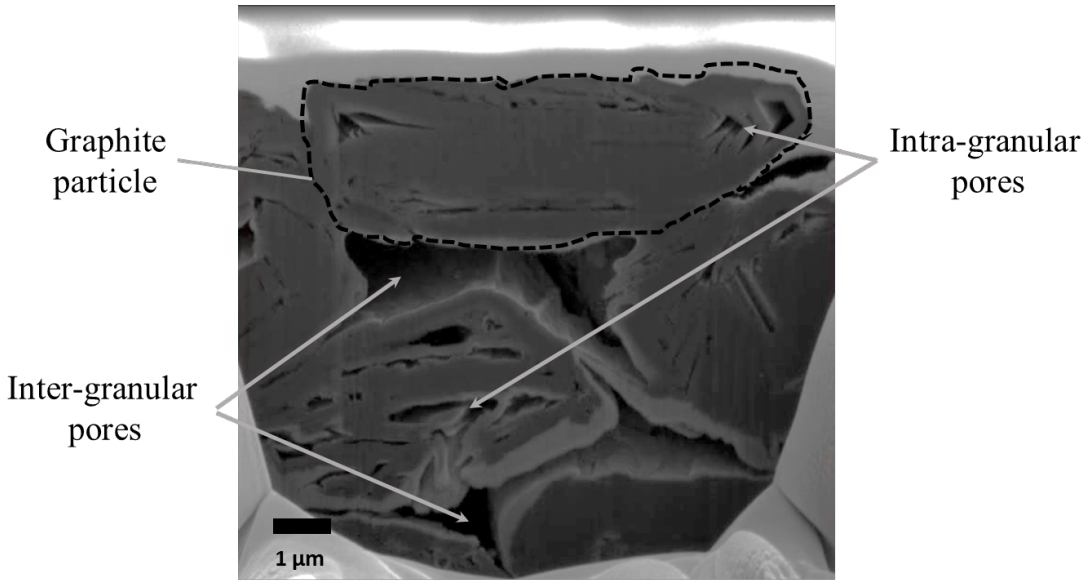

Figure 5 : SEM image showing the section of the pristine composite negative electrode. The cross section was realized by Focused Ion Beam (FIB).

Figure 5 shows the SEM image of the pristine graphite electrode. One can easily distinguish two different kinds of porosities: inter-granular pores between the different graphite particles, and intra-granular pores which is the intrinsic porosity of the graphite material. This observation of the electrode porosity helps us for the interpretation and modeling of our EIS experiments. While the common models always consider long, opened cylindrical pores, as an ideal case (semi-infinite diffusion), it is sometimes necessary to consider different alteration of the pore morphology. Actually, EIS spectra can be influenced by peculiar shape or size of pores, that can induce distortions in Li^+ diffusion path (abnormal diffusion), compared to cylinder pore model that consider only parallel diffusion paths (normal diffusion). In our case, the porosity of the negative

electrodes appears as a key parameter to be taken into account for accurate modeling of the electrode behavior, since here classical models (Warburg) are not suitable to correctly describe the electrochemical signature of the above mentioned electrodes. Existing models describing the behavior of porous electrodes were thus used as a base for the methodology developed in this paper [32,33]. Then, a modified transmission line model was used to describe the abnormal diffusion in narrow pores where the electrolyte, the SEI or insulating degradation products could be confined. It is important to precise that the limiting porosity considered in this paper only refers to intra-granular pores (nanometer scale). The inter-granular porosity (micrometer scale) is considered as large enough to maintain normal/conventional electrolyte mobility.

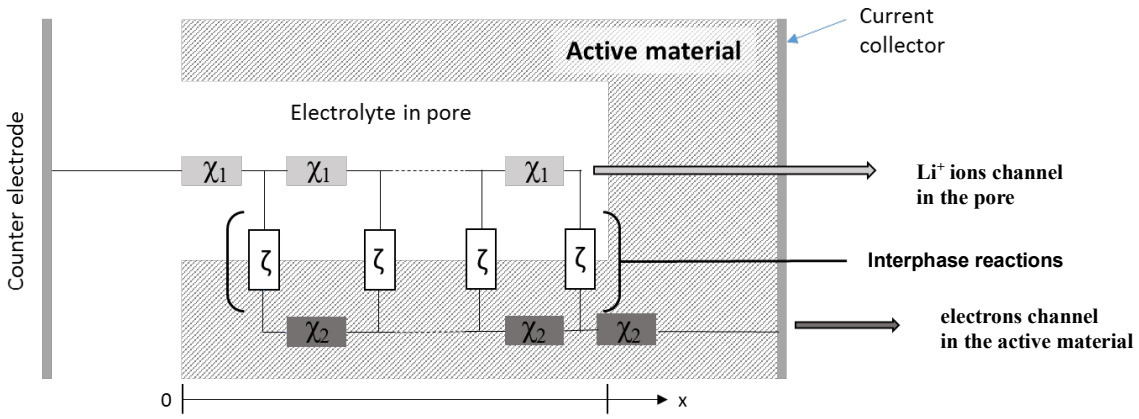

Figure 6: Schematic representation of a transmission line in a pore for the modeling of EIS spectra of graphite negative electrodes, according to De Levie model.

Figure 6 displays a schematic representation of the transmission line that can describe the electrical behavior of a porous electrode in the De Levie model [32]. This transmission line is composed of *(i)* a transversal element (ζ) to model the interactions occurring between the electrolyte in a narrow pore and the active material (giving birth to the impedance Z) and *(ii)* two parallel charge carriers transport channels (χ): one for the ionic transport in the electrolyte, confined in the narrow pores (expressed by the resistance R_s), and the other one for the electronic transport in the active material (assuming that graphite is better electronic than ionic conductor, and thus expressed by R_g). As mentioned, the active material is graphite, a material known to be very conductive. This induces a high conductivity difference between the two media (electrolyte and electrode). Thus, one can consider $R_g << R_s$. Moreover, charge transfer and double layer charge are always observed at rather high frequencies, more than 100 Hz, even for the aged electrodes. For example, storage aging

samples display a total impedance of 2,000 Ω.cm² with 1,500 Ω.cm² only due to the low frequency region, below 10 Hz. One can then consider that these phenomena are supported by the free electrolyte/electrode interface (*i.e.* in intergranular porosities, not confined in intragranular pores). The value of Z then only accounts for the confined electrolyte/electrode interface in narrow pores.

Considering these assumptions, the application at x=0 (pore entrance) of a signal for EIS measurements, which is a sinusoid voltage signal ($e = e_0 \sin(\omega t)$) with a ω angular frequency and a small value amplitude e_0, pore impedance Z_0 can be defined by:

$$Z_0 = \frac{e_0}{i_0} = \sqrt{R_s Z}\coth\left(\sqrt{\frac{R_s}{Z}}L\right) \qquad (1)$$

where L is the length of the pore.

With $Z = CPE_x = \frac{1}{Q(j\varpi)^{\alpha}}$, the electrode/electrolyte interphase is considered as blocking.

In semi-infinite conditions ($L \to \infty$), and considering $\alpha = 1$ (meaning CPE_x is a plane capacitor) the pore behaves as a Warburg element with a 45° phase shift between voltage and current. This is consistent with the comparison of the equivalent electrical circuit we used to describe a single pore and the circuit depicting the plane (normal) diffusion, which considers a R//C transmission line with a large number of elements.

As our experimental data indicate that pores seem mainly blocking, we obviously choose to fit our spectra with such an equivalent circuit (with $Z = CPE_x = \frac{1}{Q(j\varpi)^{\alpha}}$) by varying L (through the number of R,C elements in the transmission line).

Finally, terminal line impedance (depicting the electrode/collector) interface was chosen as a non-finite element ($Z_{boundary} = CPE_t = \frac{1}{Q_t(j\varpi)^{\alpha}}$) in order to take into account the frequency dispersion at low frequency. $Z_{boundary}$ is placed at the end of the resistive channel associated to the electrolyte confined in pores, to make sure that it is not in parallel nor in series with the transmission line. This way $Z_{boundary}$ has no influence on the high frequency part of the transmission line which is solely defined by volumic properties [34].

The refining of EIS spectra of Figure 4 additionally requires taking into account the passivation of the graphite surface by the SEI, as shown by XPS spectra. High frequency semi-circles in Nyquist plots of insertion electrodes usually depict the ionic conduction through the SEI. This can be modeled by a resistance connected in parallel with a capacitor, also called a R//C element. Some models consider a multilayer [35] or a mosaic-type [36] SEI requiring more than one R//C element. In this work, the SEI can be modeled by a single R//C since no noticeable depression of this semi-

circle is observed. One can then consider that this single R//C element represents an average SEI composition which is the homogenous combination of the electrical properties of all the SEI components [37].

Figure 7 displays the equivalent electrical circuit used for EIS spectra refinement, which includes the SEI contribution as well as the double layer capacitance and the charge transfer resistance, and the porosity impedance (transmission line). The resulting circuit describes quite well the electrical behavior of our aged porous negative electrodes.

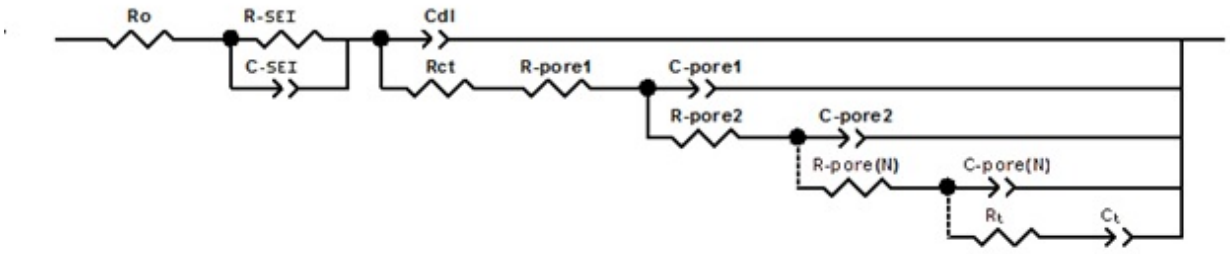

Figure 7: Equivalent circuit modeling the electrical behavior of porous negative electrode accounting for the presence of the SEI.

Penetration depth of the AC signal during EIS measurements, called μ, can be estimated according to DeLevie [32] with :

$$\mu = \frac{1}{2}\sqrt{\frac{r}{\omega \rho C_p}} \qquad (2)$$

Where r is the mean pore radius, $\rho$the electrolyte resistance and C_p the pore capacitance.

Let now λ be the maximum lithium penetration depth at constant current (I_0). λ is thus also defined as:

$$\lambda = \frac{FC_0D}{I_0} \qquad (3)$$

Assuming $\mu = \lambda$, equation (2) altogether with equation (3) in the low frequency domain (depicting abnormal diffusion between 10 Hz and 63 mHz observed in the EIS spectra) gives an idea of the maximum value of the diffusion coefficient of lithium ions in the electrolyte, confined in narrow intragranular pores. As a result, with a mean pore diameter of 100 nm (from SEM images), the diffusion coefficient is $D \sim 10^{-10}$ $cm^2.s^{-1}$. This value is 10^4 times smaller than in a fresh bulk electrolyte, considering ρ = 93.5 Ω.cm at 25°C according to Schmidt *et al.* [38] and $D \sim 2.10^{-6}$ $cm^2.s^{-1}$ [39]. This low value justifies the distortion observed in EIS spectra, in the diffusion domain.

In addition, assuming the resistivity of the electrolyte is the same as the one of SEI when it is completely filling the pores, like in storage aging case in this work, the estimated value of the lithium ions diffusion coefficient is then below 10^{-16} $cm^2.s^{-1}$.

After accelerated aging tests, the influence of the narrow porosity tends to decrease as the respective R_s values decrease dramatically. It appears that the smallest pores are filled with SEI upon aging, leading to more or less a harmonization of the pore sizes. Moreover, intense cycling contributes to open up diffusion paths, making insertion of Li^+ ions easier over cycles. Inversely, after long storage, the influence of intragranular porosities appears more noticeably (kind of semi-circle in Nyquist plots in Figure 4 and Bode plots in Figure 8, below 10 Hz).

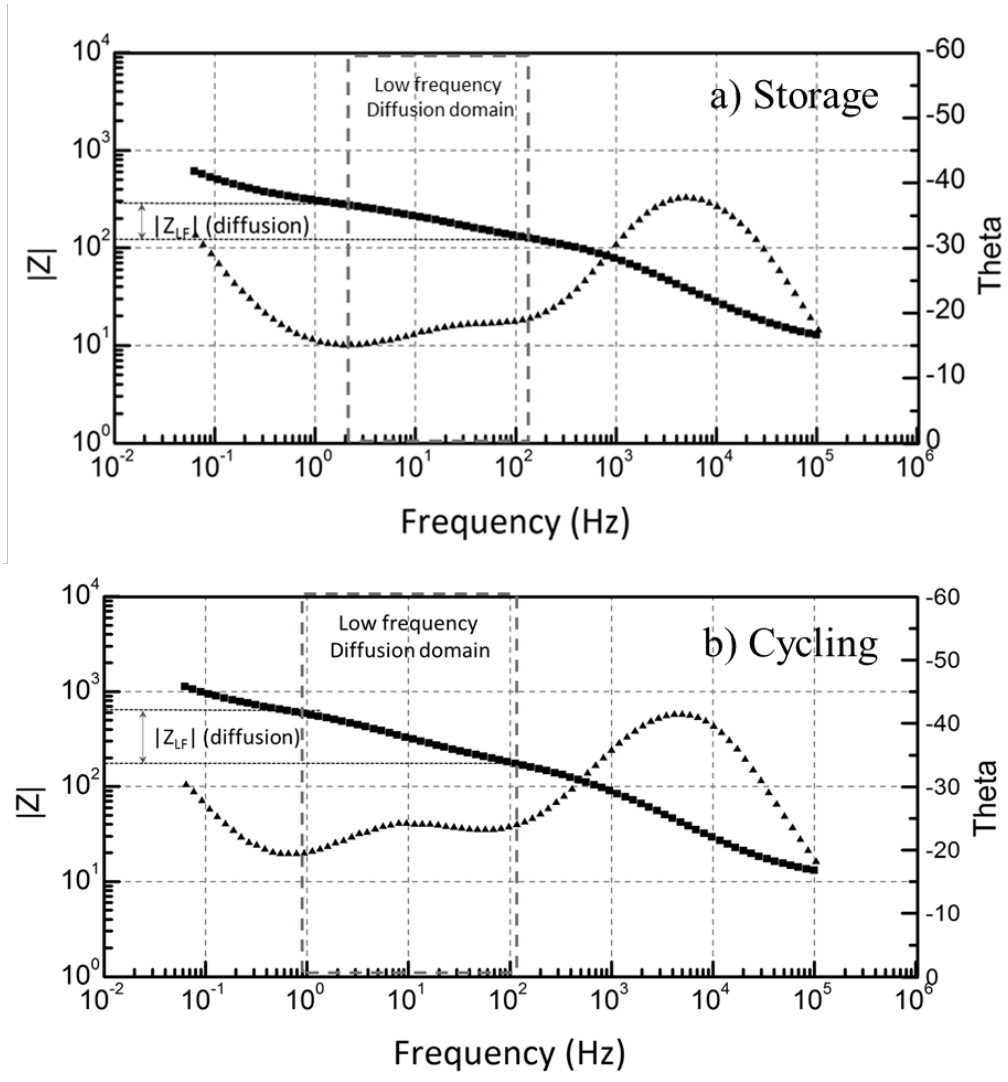

Figure 8: EIS Bode plots of graphite electrodes (a) after storage and (b) after cycling aging tests (square points stand for impedance module and triangular points stand for impedance phase).

In order to identify the origin of this important contribution, different EIS acquisitions were performed successively at different temperatures and then at different states of charge (*i.e.* lithium contents). These measurements were made by using a three-electrode cell with metallic Li as counter and reference electrode, in order to work in a defined potential range, which is not possible with the symmetrical cell configuration. The evolution of the resistance value R_{LF} (corresponding to the low frequency semi-circle) during these experiments is displayed in Figure 9.

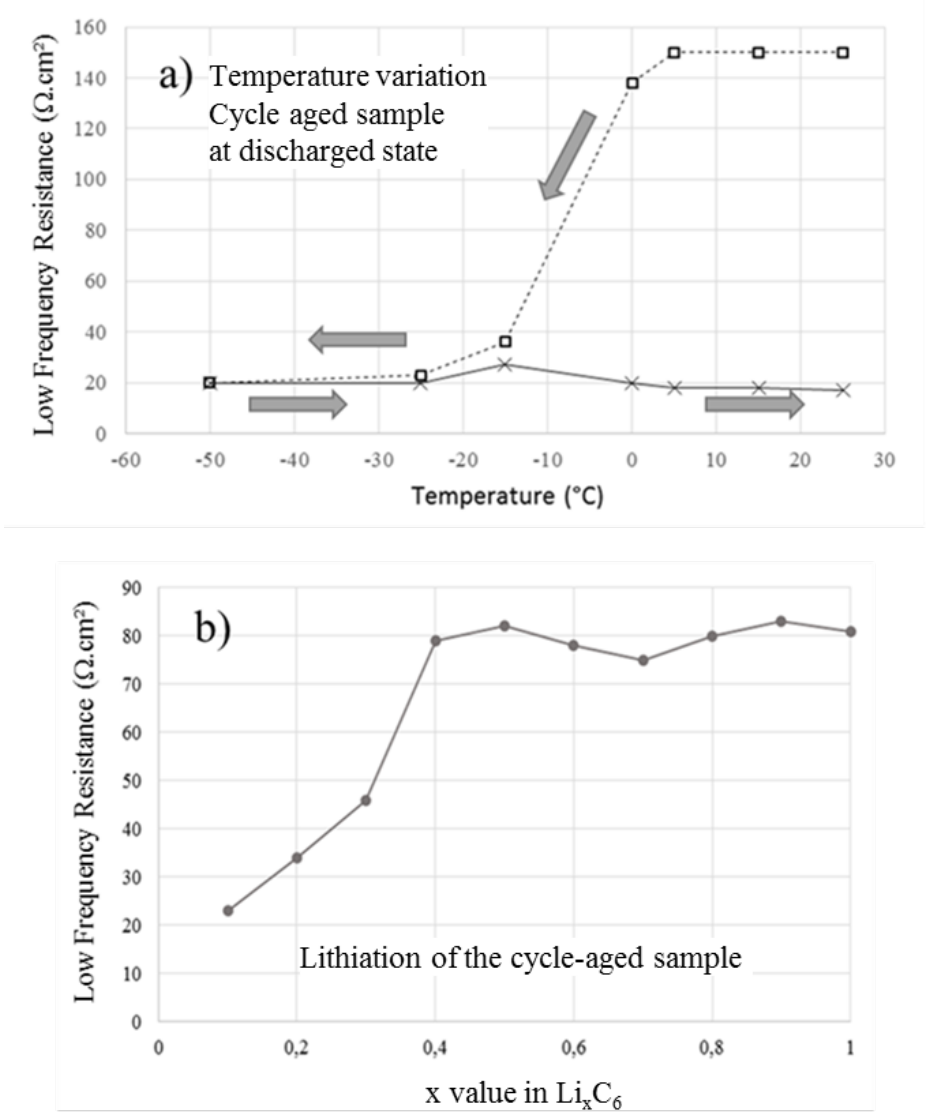

Figure 9 : Variation of the resistance R_{LF} corresponding to the low frequency semi-circle observed in Figure 4: **(a)** with temperature: dotted line for temperature decrease; solid line for the following temperature increase; **(b)** with lithium content in the graphite electrode: lithiation at C/10 of the cycling-aged electrode.

Since high temperature is a parameter known to enhance the SEI layer formation, the temperature is first decreased in order to avoid excessive SEI thickness. A first range of points performed from 25°C to -50°C show that this low frequency resistance decreases with lower temperatures, especially below -15°C, to reach a minimum of about R_{LF}= 20 Ω.cm^2. Afterwards, the temperature was increased again from -50°C to +25°C. No significant increase of the low frequency impedance (R_{LF}) was then observed. It remains at the same level for all the temperature range, meaning that this resistance variation is not reversible during this experiment. However, upon the subsequent lithiation of the same graphite sample, the low frequency resistance R_{LF} rises while the electrode is being progressively lithiated. The resistance reaches a maximum of 80 Ω.cm^2 when $x > 0.4$ in Li_xC_6.

To sum up, the low frequency contribution resistance tends to decrease at low temperature and this change is not reversible when the battery is placed at room temperature again. However, this resistance progressively increases again upon lithiation of the same sample but does not reach its initial value. To explain these variations, it is assumed that this low frequency phenomenon corresponds to the presence, in the confined SEI, of a component which *(i)* is not a good ionic conductor, and *(ii)* is more soluble in the liquid electrolyte at lower temperature. Lithium carbonate Li_2CO_3 and/or CO_2 bubbles trapped in the SEI comply well with this assumption, as their respective solubilities increase as the temperature decreases [40]. Li_2CO_3 or CO_2 bubbles can then be solubilized in the electrolyte when the temperature is below -15°C, explaining the decrease of the corresponding resistance. However, C 1s XPS spectra of graphite electrodes from cycled batteries did not display significant Li_2CO_3 quantities. It is worth noting that the typical XPS probing depth does not exceed 5 nm, which means that lithium carbonate quantity may be higher deeper in the SEI. The SEI confined in pores can then contain significantly higher amounts of Li_2CO_3 than the outermost surface, explaining that its contribution is separated from the whole SEI impedance contribution at high frequency (f ~ 8000 Hz). This hypothesis is consistent with Zaban and Aurbach [35] multi-component SEI model, stating that Li salts form a first poorly conductive inner SEI layer on the surface of the negative electrode whereas the outer SEI is mostly organic and more conductive (lower impedance).This information can be correlated with the Li_2CO_3 quantity measured after the first cycle, which can be considered as an equivalent of the “deep SEI” (*i.e.* closer to the electrode surface). Indeed, the carbonate ratio after a first cycle is significantly higher, which is in good accordance with Zaban's and Aurbach’s statement. Besides, by chemical analysis, a large amount of CO_2 is measured in the gas mixture contained in the battery after both storage and cycling aging. Carbon dioxide bubbles can then be trapped in small narrow pores of the negative electrodes, leading to an increase of the corresponding resistance, as evidenced by our EIS experiments.

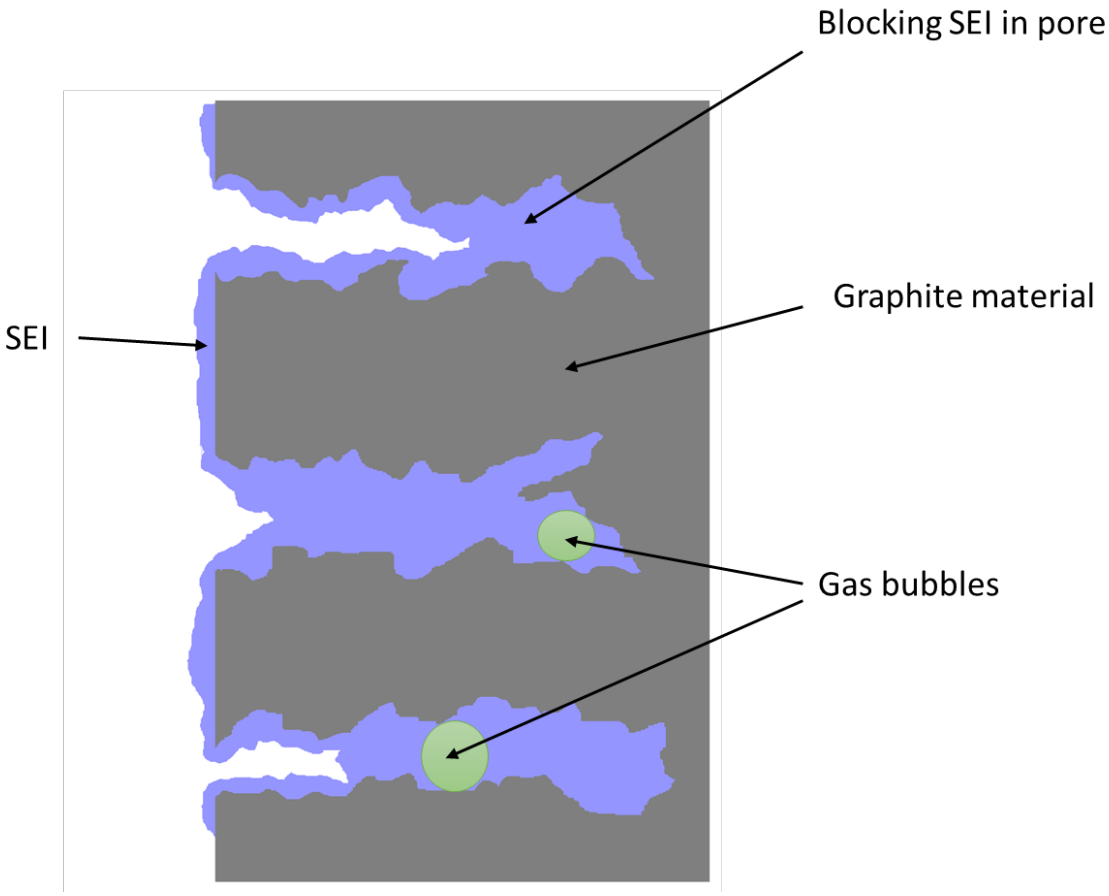

Figure 10 : Schematic representation of the partial or total filling of the pores with blocking SEI in addition with the presence of gas bubbles inside the pores

Therefore we propose the schematic view displayed in Figure 10 to describe the aging process of graphite negative electrodes, taking into account the presence of the SEI and of the electrode porosity. Partial or total filling of narrow pores by the SEI, in addition with the presence of gas bubbles inside these pores, blocks the diffusion of lithium in this porosity-type and allows interpreting our spectroscopic and electrical data. Finally, the modified transmission line derived from the De Levie model developed here evidences the crucial influence of diffusion in porous electrodes. When constrained, it induces a noticeable polarization at low frequency, below 10 Hz. It also demonstrates that the associated faradic impedance due to abnormal diffusion is mostly resistive/capacitive. This phenomenon remains however small enough (with respect to the part of blocking narrow pores involved) compared to the global impedance of the electrode and allows

good electrochemical performances of the battery. Data reported in Table 2 compare capacity loss measured after aging with the part of the global impedance of the negative electrode samples dedicated to the low frequency region.

Table 2: Capacity loss compared to the impedance part attributed to the porosity for the aged graphitic electrodes.

	3% VC		**1% VC**	
	Storage aging	**Cycling aging**	**Storage aging**	**Cycling aging**
Capacity loss	- 6%	- 6 %	- 7%	- 30 %
$\mathbf{Z_{LF}(diff.) / Z_{global}}$	20%	22%	22%	26%

The table also displays results from a battery aged in similar conditions, but with a lower VC additive concentration in the electrolyte (1%). This shows that the low frequency impedance has few or no influence on the evolution of the global capacity since the percentage representing the low frequency impedance remains quite the same for various samples while capacity loss is particularly high after cycling aging for 1% VC additive concentration in the electrolyte. For the studied batteries, this clearly enlightens the higher impact of the surface evolution (passivation and charge transfer), rather than the bulk electrode change (porosity), on the capacity fading.

4. Conclusion

Graphite negative electrode/electrolyte interfaces in Li-ion batteries have been studied after accelerated aging conditions thanks to X-ray Photoelectron Spectroscopy and Electrochemical Impedance Spectroscopy. The main aging mechanism detected here remains SEI growth (surface passivation) which could be detected by both techniques. The main contribution of this paper is that the electrical behavior of the negative electrodes is also strongly influenced by the porosity of the samples. We suggest a model describing the influence of electrochemically blocking pores. This blocking behavior is believed to be caused by confinement of lithium carbonate (Li_2CO_3) and/or gaseous CO_2 inside the narrow pores, which does not allow lithium ions to insert properly into graphite. In these pores, lithium can only participate to SEI growth, which can contribute to partially decrease the capacity by lithium consumption. But the main consequence is an outstanding perturbation of lithium diffusion in the sample. Further work is performed to improve the system performance as well as supplementary experiments to reinforce our model.

Aknowledgment

The authors thank the French National Research Agency ANR for financial support ofproject VISION (ANR-11-PRGE-0012) and Labex STORE-EX (ANR-10-LABX-0076). Mohammed BEN HASSINE, Carine DAVOISNE and Loïc DUPONT, from LRCS (UMR 7314 CNRS) in Amiens, France are warmly thanked for Focused Ion Beam (FIB) - electron microscopy images and fruitful discussions.

References

[1] P. Denholm, R.M. Margolis, Evaluating the limits of solar photovoltaics (PV) in traditional electric power systems, *Energy Policy***35** (2007) 2852-2861

[2] T. Kousksou, P. Bruel, A. Jamil, T. El Rhafiki, Y. Zeraouli, Energy storage: Applications and challenges, *Sol. Energy Mater. Sol. Cells* 120 (2014) 59–80

[3] A. Poullikkas, A comparative overview of large-scale battery systems for electricity storage, Renew. Sustain. Energy Rev. 27 (2013) 778–788

[4] K.C. Divya, J. Ostergraad, Battery energy storage technology for power systems-An overview, Electr. Power Syst. Res. 79 (2009) 511–520

[5] R.F. Nelson, Power requirements for batteries in hybrid electric vehicles, J. Power Sources. 91 (2000) 2–26

[6] G. Sarre, P. Blanchard, M. Broussely, Aging of lithium-ion batteries, J. Power Sources. 127 (2004) 65–71

[7] A. Purvins, I.T. Papaioannou, L. Debarberis, Application of battery-based storage systems in household-demand smoothening in electricity-distribution grids, Energy Convers. Manag. 65 (2013) 272–284

[8] J. Leadbetter, L.G. Swan, Selection of battery technology to support grid-integrated renewable electricity, J. Power Sources. 216 (2012) 376–386

[9] J. Vetter, P. Novák, M.R. Wagner, C. Veit, K.-C. Möller, J.O. Besenhard, et al., Ageing mechanisms in lithium-ion batteries, J. Power Sources. 147 (2005) 269–281

[10] M. Broussely, P. Biensan, F. Bonhomme, P. Blanchard, S. Herreyre, K. Nechev, et al., Main aging mechanisms in Li ion batteries, J. Power Sources. 146 (2005) 90–96

[11] J. Li, E. Murphy, J. Winnick, P.A. Kohl, Studies on the cycle life of commercial lithium ion batteries during rapid charge–discharge cycling, J. Power Sources. 102 (2001) 294–301

[12] G. Amatucci, J.-M. Tarascon, L.. Klein, Cobalt dissolution in LiCoO2-based non-aqueous rechargeable batteries, Solid State Ion. 83 (1996) 167–173

[13] S. Verdier, L. El Ouatani, R. Dedryvère, F. Bonhomme, P. Biensan, D. Gonbeau, XPS study on Al_2O_3- and $AlPO_4$-coated $LiCoO_2$ cathode material for high-capacity Li ion batteries, J. Electrochem. Soc. 154 (2007) A1088–A1099

[14] J.W. Braithwaite, A. Gonzales, G. Nagasubramanian, S.J. Lucero, D.E. Peebles, J.A. Ohlhausen, et al., Corrosion of Lithium ‐ Ion Battery Current Collectors, J. Electrochem. Soc. 146 (1999) 448–456

[15] V. Agubra, J. Fergus, Lithium Ion Battery Anode Aging Mechanisms, Materials. 6 (2013) 1310–1325

[16] C. Wang, A.J. Appleby, F.E. Little, Charge–discharge stability of graphite anodes for lithium-ion batteries, J. Electroanal. Chem. 497 (2001) 33–46

[17] E. Radvanyi, K. Van Havenbergh, W. Porcher, S. Jouanneau, J.-S. Bridel, S. Put, S. Franger, Study and modelling of the solid electrolyte interphase behaviour on nano-silicon anodes by EIS, Electrochimica Acta, 137 (2014) 751.

[18] T. Yoshida, M. Takahashi, S. Morikawa, C. Ihara, H. Katsukawa, T. Shiratsuchi, et al., Degradation Mechanism and Life Prediction of Lithium-Ion Batteries, J. Electrochem. Soc. 153 (2006) A576–A582

[19] C. Dudézert, PhD thesis, University Paris Sud, 2009

[20] Q. Badey, PhD thesis, University Paris Sud, 2011

[21] Q. Badey, G. Cherouvrier, Y. Reynier, J.-M. Duffault, S. Franger, Ageing forecast of lithium-ion batteries for electric and hybrid vehicles, Curr. Top. Electrochem. 16 (2011) 65–79

[22] M. Safari, M. Morcrette, A. Teyssot, C. Delacourt, Life-Prediction Methods for Lithium-Ion Batteries Derived from a Fatigue Approach I. Introduction: Capacity-Loss Prediction Based

on Damage Accumulation, J. Electrochem. Soc. 157 (2010) A713–A720
[23] M. Safari, M. Morcrette, A. Teyssot, C. Delacourt, Life Prediction Methods for Lithium-Ion Batteries Derived from a Fatigue Approach II. Capacity-Loss Prediction of Batteries Subjected to Complex Current Profiles, J. Electrochem. Soc. 157 (2010) A892–A898
[24] M. Ecker, J.B. Gerschler, J. Vogel, S. Käbitz, F. Hust, P. Dechent, et al., Development of a lifetime prediction model for lithium-ion batteries based on extended accelerated aging test data, J. Power Sources. 215 (2012) 248–257
[25] G.K. Prasad, C.D. Rahn, Model based identification of aging parameters in lithium ion batteries, J. Power Sources. 232 (2013) 79–85
[26] S. Santhanagopalan, Q. Guo, P. Ramadass, R.E. White, Review of models for predicting the cycling performance of lithium ion batteries, J. Power Sources. 156 (2006) 620–628
[27] A. Barré, B. Deguilhem, S. Grolleau, M. Gérard, F. Suard, D. Riu, A review on lithium-ion battery ageing mechanisms and estimations for automotive applications, J. Power Sources. 241 (2013) 680–689
[28] L. El Ouatani, R. Dedryvère, J.-B. Ledeuil, C. Siret, P. Biensan, J. Desbrières, et al., Surface film formation on a carbonaceous electrode: Influence of the binder chemistry, J. Power Sources. 189 (2009) 72–80
[29] S. Leroy, F. Blanchard, R. Dedryvère, H. Martinez, B. Carré, D. Lemordant, et al., Surface film formation on a graphite electrode in Li-ion batteries: AFM and XPS study, Surf. Interface Anal. 37 (2005) 773–781
[30] R. Dedryvère, S. Laruelle, S. Grugeon, L. Gireaud, J.-M. Tarascon, D. Gonbeau, XPS Identification of the Organic and Inorganic Components of the Electrode/Electrolyte Interface Formed on a Metallic Cathode, J. Electrochem. Soc. 152 (2005) A689–A696
[31] L. El Ouatani, R. Dedryvère, C. Siret, P. Biensan, S. Reynaud, P. Iratçabal, et al., The Effect of Vinylene Carbonate Additive on Surface Film Formation on Both Electrodes in Li-Ion Batteries, J. Electrochem. Soc. 156 (2009) A103
[32] R. De Levie, Electrochemical Responses of Porous and Rough Electrodes, in: Adv. Electrochem. Electrochem. Eng., Wiley Interscience Ed., P. Delahay, New York, 1967: pp. 329–397
[33] E. Radvanyi, W. Porcher, E. De Vito, A. Montani, S. Franger, S. Jouanneau Si Larbi, Failure mechanisms of nano-silicon anodes upon cycling: an electrode porosity evolution model. *Phys. Chem. Chem. Phys.* 16 (2014) 17142-17153.
[34] J. Bisquert, Influence of the boundaries in the impedance of porous film electrodes, *Phys. Chem. Chem. Phys.* 2 (2000) 4185–4192
[35] A. Zaban, D. Aurbach, Impedance spectroscopy of lithium and nickel electrodes in propylene carbonate solutions of different lithium salts A comparative study, J. Power Sources. 54 (1995) 289–295
[36] E. Peled, D. Golodnitsky, G. Ardel, Advanced model for solid electrolyte interphase electrodes in liquid and polymer electrolytes, J. Electrochem. Soc. 144 (1997) L208–L210
[37] J. Thevenin, R. Muller, Impedance of lithium electrodes in a propylene carbonate electrolyte, J. Electrochem. Soc. 134 (1987) 273–280
[38] M. Schmidt, U. Heider, A. Kuehner, R. Oesten, M. Jungnitz, N. Ignat'ev, et al., Lithium fluoroalkylphosphates: a new class of conducting salts for electrolytes for high energy lithium-ion batteries, J. Power Sources. 97-98 (2001) 557–560
[39] L. Ole Valoen, J. Reimers, Data obtained from E-one Moli Energy (Canada), (n.d.)
[40] W. Yi, C. Yan, P. Ma, F. Li, X. Wen, Refining of crude Li_2CO_3 via slurry phase dissolution using CO_2, Sep. Purif. Technol. 56 (2007) 241–248